First Stage of Thermal Aging under Oxidizing Conditions of a $Ce_{0.62}Zr_{0.38}O_2$ Mixed Oxide with an Ordered Cationic Sublattice: A Chemical, Nanostructural, and Nanoanalytical Study

María P. Yeste, Juan C. Hernández, Susana Trasobares, Serafín Bernal,* Ginesa Blanco, José J. Calvino, José A. Pérez-Omil, and José M. Pintado

Departamento de Ciencia de los Materiales e Ingeniería Metalúrgica y Química Inorgánica, Facultad de Ciencias, Universidad de Cádiz, Campus Rio San Pedro, Puerto Real, E-11510-Cádiz, Spain

Received April 1, 2008. Revised Manuscript Received May 13, 2008

After being heated in a flow of 5% O_2/He, at 1073 or 1123 K for 30 min, a $Ce_{0.62}Zr_{0.38}O_2$ sample showing an ordered cationic sublattice had very subtle surface nanostructural changes induced on it. In parallel with them, a significant loss of low-temperature ($T \leq 773$ K) oxygen storage capacity (OSC), with no modification of its high-temperature ($T \geq 973$ K) redox response, was observed. These nanostructural and chemical features characterize the very first stage of the process leading to the destruction of the ordered Ce−Zr sublattice, a structural phenomenon playing a key role in the control of redox behavior of ceria−zirconia mixed oxides. The reported results, including OSC, hydrogen chemisorption, and nanostructural and nanoanalytical data, lend further support to a model providing a comprehensive interpretation of the complex relationship linking thermal aging conditions, nanostructural properties, surface chemistry, and redox behavior in these materials.

Introduction

The reversible changes of redox behavior observed in ceria−zirconia mixed oxides by the application of appropriate thermal aging pretreatments is a very characteristic and puzzling feature of their chemistry.[1–8] Although some other interpretations have been proposed in the literature,[9–14] there are presently numerous experimental results that suggest the existence of a close relationship between the structural changes occurring in the oxides and the modifications observed in their redox properties. These structural changes mainly consist of the formation/destruction of an ordered, pyrochlore-related, cationic Ce−Zr sublattice.[1,2,5,7,8,14–21] Enhanced reducibility is observed in samples exhibiting an ordered arrangement of cations.[1,2,5–8,15,19–23]This phase is known to be typically formed by the successive application of a severe reduction treatment to the Ce−Zr mixed oxide (SR; $T_{redn} \geq 1173$ K) and a mild reoxidation (MO, $T_{reoxn} \leq 873$ K). In this way, the so-called CZ-MO sample, with a pyrochlore-related ordered structure,[1,2,21] is obtained.[1,5–7,17–20,22] By contrast, associated with the oxide phase showing a disordered distribution in its cationic sublattice, a significant loss of oxygen storage capacity (OSC) is observed.[2,5–8,20] This disordered Ce−Zr distribution typically results from the application of a high-temperature oxidizing treatment (severe oxidation, SO, $T_{reoxn} \geq 1173$ K),[2,5–8,20] a CZ-SO type of sample.[20]

* Corresponding author. Tel.: +34-956-016338; fax: +34-956-016288; e-mail: serafin.bernal@uca.es.

(1) Izu, N.; Omata, T.; Otsuka-Yao-Matsuo, S. *J. Alloys Compd.* **1998**, *270*, 107.
(2) Otsuka-Yao-Matsuo, S.; Omata, T.; Izu, N.; Kishimoto, H. *J. Solid State Chem.* **1998**, *138*, 47.
(3) Baker, R. T.; Bernal, S.; Blanco, G.; Cordón, A. M.; Pintado, J. M.; Rodríguez-Izquierdo, J. M.; Fally, F.; Perrichon, V. *Chem. Commun. (Cambridge, U.K.)* **1999**, 149.
(4) Fornasiero, P.; Montini, T.; Graziani, M.; Kaspar, J.; Hungría, A. B.; Martínez-Arias, A.; Conesa, J. C. *Phys. Chem. Chem. Phys.* **2002**, *4*, 149.
(5) Suda, A.; Ukyo, Y.; Yamamura, K.; Sobukawa, H.; Sasaki, T.; Nagai, Y.; Tanabe, T.; Sugiura, M. J. *Ceram. Soc. Jpn.* **2004**, *112*, 586.
(6) Montini, T.; Hickey, N.; Fornasiero, P.; Graziani, M.; Bañares, M. A.; Martínez-Huerta, M. V.; Alessandri, I.; Depero, L. E. *Chem. Mater.* **2005**, *17*, 1157.
(7) Alessandri, I.; Bañares, M. A.; Depero, L. E.; Ferroni, M.; Fornasiero, P.; Gennari, F. C.; Hickey, N.; Martinez-Huerta, M. V.; Montini, T. *Top. Catal.* **2006**, *41*, 35.
(8) Zhao, M.; Shen, M.; Wang, J. *J. Catal.* **2007**, *248*, 258.
(9) Mamontov, E.; Brezny, R.; Koranne, M.; Egami, T. *J. Phys. Chem. B* **2003**, *107*, 13007.
(10) Mamontov, E.; Egami, T.; Brezny, R.; Koranne, M.; Tyagi, S. *J. Phys. Chem. B* **2000**, *104*, 11110.
(11) Wang, R.; Crozier, P. A.; Sharma, R.; Adams, J. B. *J. Phys. Chem. B* **2006**, *110*, 18278.
(12) Putna, E. S.; Bunluesin, T.; Fan, X. L.; Gorte, R. J.; Vohs, J. M.; Lakis, R. E.; Egami, T. *Catal. Today* **1999**, *50*, 343.
(13) Costa-Nunes, O.; Gorte, R. G.; Vohs, J. M. *J. Mater. Chem.* **2005**, *15*, 1520.
(14) Costa-Nunes, O.; Ferrizz, R. M.; Gorte, R. J.; Vohs, J. M. *Surf. Sci.* **2005**, *592*, 8.
(15) Montini, T.; Bañares, M. A.; Hickey, N.; Di Monte, R.; Fornasiero, P.; Kaspar, J.; Graziani, M. *Phys. Chem. Chem. Phys.* **2004**, *6*, 1.
(16) Pérez Omil, J. A.; Bernal, S.; Calvino, J. J.; Hernández, J. C.; Mira, C.; Rodríguez-Luque, M. P.; Erni, R.; Browning, N. D. *Chem. Mater.* **2005**, *17*, 4282.
(17) Sasaki, T.; Ukyo, Y.; Kuroda, K.; Arai, S.; Saka, H. *J. Electron Microsc.* **2003**, *52*, 309.
(18) Sasaki, T.; Ukyo, Y.; Suda, A.; Sugiura, M.; Kuroda, K.; Arai, S.; Saka, H. J. *Ceram. Soc. Jpn.* **2003**, *111*, 382.
(19) Izu, N.; Kishimoto, H.; Omata, T.; Yao, T.; Otsuka-Yao-Matsuo, S. *Sci. Technol. Adv. Mater.* **2001**, *2*, 443.
(20) Yeste, M. P.; Hernández, J. C.; Bernal, S.; Blanco, G.; Calvino, J. J.; Pérez-Omil, J. A.; Pintado, J. M. *Chem. Mater.* **2006**, *18*, 2750.
(21) Izu, N.; Kishimoto, H.; Omata, T.; Yao, T.; Otsuka-Yao-Matsuo, S. *Sci. Technol. Adv. Mater.* **2001**, *2*, 397.
(22) Hernández, J. C.; Hungría, A. B.; Pérez-Omil, J. A.; Trasobares, S.; Bernal, S.; Midgley, P. A.; Alavi, A.; Calvino, J. J. *J. Phys. Chem. C* **2007**, *111*, 9001.
(23) Kishimoto, H.; Omata, T.; Otsuka-Yao-Matsuo, S.; Ueda, K.; Hosono, H.; Kawazoe, H. *J. Alloys Compd.* **2000**, *312*, 94.

10.1021/cm800928p CCC: $40.75
Published on Web 07/04/2008

As discussed in some recent papers,[7,20,24] the relationship existing between nanostructural properties and redox response of these materials is complex. In the low-temperature domain, typically $T \leq 773$ K, kinetic factors related to the capability of oxide surfaces to activate the dissociative chemisorption of the hydrogen molecule would be the key controlling factors.[20] Accordingly, a low-temperature redox response would be very dependent on the surface structure of the aged oxides, the one associated with an ordered arrangement of Ce−Zr cations showing the highest rate for hydrogen chemisorption.[20] By contrast, in the high-temperature region, typically $T \geq 973$ K, the redox response would be determined by the thermodynamic properties of the corresponding oxide and therefore mainly depends on their bulk structural properties.[20] In good agreement with earlier studies,[5,17,19] in ref 20, it was proposed that the CZ-MO sample (ordered Ce−Zr sublattice) exhibited a higher thermodynamic reducibility than the CZ-SO sample. We may conclude, accordingly, that the pyrochlore-related phase showed both the highest capability for hydrogen activation and the highest intrinsic thermodynamic reducibility. However, the nature of factors controlling the low- and high-temperature redox response in ceria−zirconia mixed oxides is very different.[20]

In addition to chemical[20] and nanostructural[16,20,22] studies characterizing the CZ-MO and CZ-SO samples (i.e., oxides exhibiting extreme redox behaviors), in ref 20, an additional sample was prepared by the reduction of CZ-SO in a flow of 5% H_2/Ar, for 1 h at 1223 K, and further reoxidation under mild conditions. This oxide, which is referred to as CZ-SO-H1223, shows high-temperature OSC values very close to those of CZ-SO but significantly improved low-temperature reducibility. Likewise, the high-resolution electron microscopy (HREM) images recorded for this sample evidenced the surface reconstruction of the pyrochlore-type ordered phase. This sample, whose behavior also can be explained in terms of the interpretation suggested previously for CZ-MO and CZ-SO, therefore characterizes the intermediate state of the oxide in the disorder−order (CZ-SO → CZ-MO) transition process.

In accordance with the reversible nature of the changes observed in ceria−zirconia mixed oxides, investigation of the first stage of the order−disorder process transforming the CZ-MO sample into the CZ-SO sample is interesting. The information gained for this process, which has not been studied in detail as yet, allows us to complete chemical and nanostructural characterization of ceria−zirconia states occurring throughout the whole reversible cycle. For this purpose, two additional samples, which will be referred to as CZ-MO-O1073 and CZ-MO-O1123, were prepared by applying short thermal aging treatments to the CZ-MO oxide, under oxidizing conditions, at either 1073 or 1123 K, two temperatures below the limit at which the massive CZ-MO → CZ-SO phase transition takes place. The investigation of these two samples included chemical, ultimate OSC, hydrogen volumetric adsorption, nanostructural, HREM, and nanoanalytical, scanning–transmission electron microscopy–X-ray energy dipersive spectroscopy (STEM-XEDS), characterization studies. As will be discussed, the results presented in this work are fully consistent with those reported in earlier studies from our laboratory on this topic,[16,20,22,24] thus giving further substantial support to the proposal of a comprehensive model correlating thermal aging conditions, nanostructural properties, surface chemistry, and redox behavior of ceria−zirconia mixed oxides.

Experimental Procedures

The two $Ce_{0.62}Zr_{0.38}O_2$ mixed oxides used as reference materials in this study were the same as already investigated in ref 20. They will be referred to as CZ-MO and CZ-SO. They were obtained by applying to two aliquots of 25 g of a commercial low-surface area (SBET: 19 $m^2\ g^{-1}$) sample (CZ-LS) from Grace Davison a common SR treatment consisting of their heating, in a flow of pure hydrogen of 500 $cm^3\ min^{-1}$, at 5 K min^{-1}, up to 1223 K, followed by 5 h of isothermal treatment at 1223 K. Always at 1223 K the samples were flushed with pure He (500 $cm^3\ min^{-1}$) for 1 h and then cooled to 298 K under inert gas flow. After completing this step, two different reoxidation routines were applied to each of the aliquots. One of them was heated in a flow of O_2(5%)/He (500 $cm^3\ min^{-1}$) at 773 K (1 h), MO step, thus resulting in the CZ-MO sample, with a BET surface area of 16 $m^2\ g^{-1}$. The other one was reoxidized in a flow of pure O_2 (500 $cm^3\ min^{-1}$) at 1223 K (5 h), SO step, thus obtaining the CZ-SO sample, with a BET surface area of 12 $m^2\ g^{-1}$. In both cases (MO and SO treatments), prior to starting the heating reoxidation program, the reduced samples were pulsed with 5% O_2/He at room temperature, to avoid uncontrolled overheating of the oxides. Starting from the CZ-MO mixed oxide, two additional samples, hereafter referred to as CZ-MO-O1073 and CZ-MO-O1123, were prepared. They resulted from the application of a 30 min thermal aging treatment to CZ-MO, in a flow of 5% O_2/He at either 1073 or 1123 K, followed by cooling to 298 K, always under flowing 5%O_2/He.

To characterize the redox behavior of the previously mentioned oxides, ultimate OSC data, as understood in refs 25–28, were determined by either thermogravimetric analysis[5] or volumetric chemisorption of O_2.[20] In the first case, data were recorded on a TA thermobalance, model Q-600. Typically, 100 mg of the oxide samples was successively heated in a stepwise manner at 473 K (1 h), 623 K (1 h), 773 K (1 h), 973 K (1 h), 1173 K (1 h), and 1223 K (1 h), at a flow of 60 $cm^3\ min^{-1}$ of 5% H_2/Ar ($P(H_2) = 38$ Torr). The heating rate between successive isothermal steps was always 10 K min^{-1}. The ultimate OSC data were determined from the corresponding weight loss recorded after completing each of the 1 h isothermal steps of the program. In accordance with the results obtained in parallel temperature programmed reduction-mass spectrometry experiments, it was assumed that the only significant weight loss during the reduction treatments was due to oxygen abstraction from the oxide lattices.

Regarding the ultimate OSC data determined from oxygen volumetric chemisorption,[20] 200 mg of the oxide samples was first reduced in a flow of 60 $cm^3\ min^{-1}$ of 5% H_2/Ar for 1 h at each of

(24) Bernal, S.; Blanco, G.; Calvino, J. J.; Hernández, J. C.; Pérez-Omil, J. A.; Pintado, J. M.; Yeste, M. P. *J. Alloys Compd.* **2008**, *451*, 521.
(25) Duprez, D.; Descorme, C. In *Catalysis by Ceria and Related Materials*; Trovarelli, A., Ed.; Imperial College Press: London, 2002; Ch. 7, pp 243−280.
(26) Aneggi, E.; Boaro, M.; de Leitenburg, C.; Dolcetti, G.; Trovarelli, A. *J. Alloys Compd.* **2006**, *408−412*, 1096.
(27) Vidal, H.; Kaspar, J.; Pijolat, M.; Colón, G.; Bernal, S.; Cordón, A.; Perrichon, V.; Fally, F. *Appl. Catal., B* **2001**, *30*, 75.
(28) Vidal, H.; Bernal, S.; Kaspar, J.; Pijolat, M.; Perrichon, V.; Blanco, G.; Pintado, J. M.; Baker, R. T.; Colón, G.; Fally, F. *Catal. Today* **1999**, *54*, 93.

the temperatures mentioned previously. The heating ramp was always 10 K min^{-1}. Then, they were evacuated (residual pressure $<1 \times 10^{-6}$ Torr) for 1 h at the reduction temperature, or 773 K if $T_{redn} \leq 773$ K, and finally reoxidized at 473 K by means of O_2 isotherms recorded on a Micromeritics, model ASAP 2020, instrument. The oxygen partial pressure interval was 0−300 Torr. Examples of the recorded isotherms may be found elsewhere.[20] Prior to all OSC determinations, the samples were heated in a flow of 5% O_2/He (60 cm^3 min^{-1}), at 773 K (1 h), and then they were cooled to 398 K under the same gas flow and finally to 298 K in a flow of He.

The hydrogen chemisorption studies of CZ-MO-O1123 K were performed by using a volumetric technique. The experimental protocol was the same as that used in ref 20. In brief, the oxide sample was first cleaned by the standard oxidizing pretreatment at 773 K as described previously. The only difference was the use of dynamic high vacuum, instead of flowing He, in the final cooling step from 398 to 298 K. The sample was then treated with 38 Torr of H_2, at 298 K, and successively heated for 30 min at 373, 423, 448, 473, 523, and 573 K, followed in every case by cooling to 298 K under hydrogen pressure. The amount of hydrogen chemisorbed after each of these heating−cooling cycles was determined from the observed hydrogen pressure drop.

HREM and energy dispersive X-ray spectroscopy (XEDS) studies were performed on a JEOL 2010-FEG 200 kV Schottky field emission TEM-STEM instrument, with a structural resolution of 0.19 nm. This microscope also was equipped with an Oxford XEDS analyzer. Electron microscopy specimens were prepared by depositing the oxide samples on lacy carbon coated 3 mm Cu grids. To avoid any contact with solvents, deposition was achieved by dipping the grids directly into the powder samples and then blowing off the excess.

Structural analysis of the recorded images was performed by using the Digital Micrograph 3.4.3 suite from Gatan. The digital diffraction patterns (DDPs) reported here correspond to the log-scaled power spectrum of the corresponding fast Fourier transforms. The XEDS spectra were recorded with a 2 nm probe size. The spectra were further processed with the help of INCA software, version 4.05, from Oxford Instruments.

Results and Discussion

Redox (OSC) Characterization Studies. Table 1 and Figure 1 summarize the ultimate OSC data determined for CZ-MO, CZ-SO (i.e., oxides with extreme redox responses), and for samples resulting from 30 min oxidizing treatments to CZ-MO at either 1073 K (CZ-MO-O1073) or 1123 K (CZ-MO-O1123). Data corresponding to CZ-SO-H1223 (i.e., sample obtained by CZ-SO reduction treatment in a flow of 5% H_2/Ar, at 1223 K (1 h), followed by reoxidation with 5% O_2/He at 773 K (1 h)) also are included in Table 1, for comparison. As explained in the Experimental Procedures, the OSC data reported in Table 1 and Figure 1 all were determined by applying 1 h reduction under flowing 5% H_2/Ar at each of the indicated temperatures.

Regarding the redox response of CZ-MO (ordered cationic sublattice) and CZ-SO (disordered cationic sublattice) mixed oxides, Table 1 and Figure 1 clearly show that the CZ-MO sample exhibits the best reducibility throughout the whole range of temperatures. As already stressed, however, a critically important distinction should be made between the origin of the observed differences in the low- ($T \leq 773$ K) and high-temperature ($T \geq 973$ K) ranges, kinetic in the former case and thermodynamic in the latter.[20] This conclusion was drawn from comparative analysis of OSC data recorded for the bare CZ-MO and CZ-SO mixed oxides and the corresponding oxide-supported Rh samples. As shown in ref 20 in the low-temperature range ($T \leq 773$ K), the OSC values for Rh/CZ-MO and Rh/CZ-SO samples are much larger than those determined for the bare oxides. This remarkable difference was interpreted as due to the catalytic effect of the supported metal phase. In the presence of a highly dispersed metal, an alternative, much faster, mechanism of H_2 adsorption on the oxides may occur. This mechanism consists of the dissociation of H_2 over the metal nanoparticles, followed by transfer of H atoms onto the oxide supports via a spillover process.[29–32] In this way, at $T \leq 773$ K, the overall oxide reduction process is much faster on the Rh containing samples, thus explaining the larger OSC values recorded for them. It was concluded in ref 20 that, in the low-temperature range, for the bare oxide samples, the OSC values were determined by kinetic factors, the rate controlling step being the hydrogen adsorption process. By contrast, at $T \geq 973$ K, no influence of the supported Rh

Table 1. Ultimate H_2-OSC Data Corresponding to a Series of Ce−Zr Mixed Oxides Prepared by Application of Different Thermal Aging Pretreatments to the Same $Ce_{0.62}Zr_{0.38}O_2$ Sample

	ultimate OSC (data expressed as percentage of total Ce^{4+} reduced to Ce^{3+})				
reduction temp (K)	CZ-MO[a] (%)	CZ-MO-O1073[a] (%)	CZ-MO-O1123[b] (%)	CZ-SO[a] (%)	CZ-SO-H1223[a] (%)
473	8	2	2	0	
623	45	22	10	3	15
773	63	61	46	17	45
973	74	73	73	50	
1173	81	81	81	62	
1223	82	82	82	69	70

[a] OSC data as determined by volumetric chemisorption of O_2, $P(O_2) = 300$ Torr, at 473 K. Oxide samples prereduced with flowing 5% H_2/Ar, for 1 h, at the indicated temperatures. Data for samples CZ-MO, CZ-SO, and CZ-SO-H1223 K were taken from ref 20. Further details of experimental protocol may be found in ref 20. [b] OSC data as determined by stepwise thermogravimetric analysis. The sample was first submitted to a cleaning pretreatment consisting of its heating in a flow of 5% O_2/He, at 773 K (1 h), followed by cooling to 398 K under the same atmosphere. Then the gas flow was switched to pure He, and the sample was cooled to 298 K. Finally, the gas flow was switched to 5% H_2/Ar, and the temperature was stepwise increased to 473, 623, 773, 973, 1173, and 1223 K; duration of the isothermal steps was 1 h.

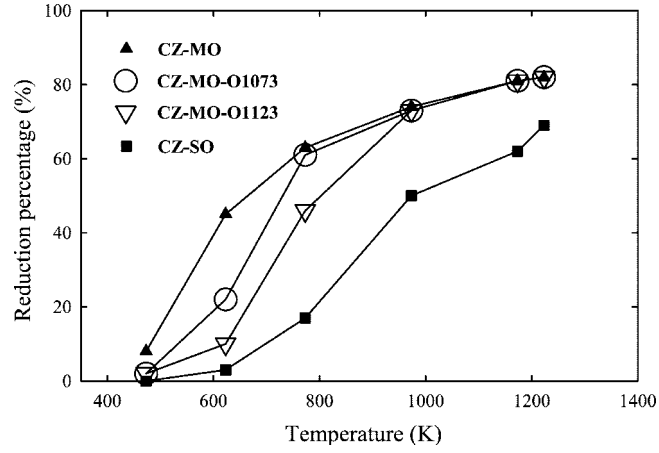

Figure 1. Evolution with temperature of ultimate H_2-OSC data for CZ-MO, CZ-MO-O1073, CZ-MO-O1123, and CZ-SO.

phase on the OSC data was observed.[20] It was concluded, accordingly, in the high-temperature range, that hydrogen adsorption on the bare oxides is fast enough as not to represent a controlling factor; the OSC values therefore were determined by thermodynamic properties of the corresponding oxides.[20]

In accordance with OSC data reported for CZ-MO-O1073 and CZ-MO-O1123, the additional oxidizing treatments applied to the CZ-MO sample induced a significant deterioration of its low-temperature reducibility, with no parallel modification of the high-temperature behavior. This is a remarkable observation that clearly suggests that these treatments have substantially modified the hydrogen activation capability of the CZ-MO sample (i.e., the surface structure) without affecting its bulk structural properties and, therefore, the thermodynamics of the reduction process.[20] Moreover, the comparison of the low-temperature OSC data recorded for CZ-MO-O1073 and CZ-MO-O1123 in Figure 1 indicates the progressive nature of this surface modification, as the temperature of the oxidizing pretreatment is increased from 1073 to 1123 K. We should conclude, accordingly, that the observed effects correspond to the very first stages of the process transforming the ordered, pyrochlore-related phase into the CZ-SO phase. Likewise, the results suggest that this process starts at the surface of the CZ-MO mixed oxide.

Hydrogen Chemisorption Studies. Changes in the low-temperature OSC response may be related to surface modifications affecting the oxide capability for activating the hydrogen molecule.[20,22,24] Accordingly, it seemed interesting to run an additional experiment aimed at investigating the behavior of the CZ-MO-O1123 sample against H_2 chemisorption. Figure 2 reports the results of this particular experiment. Also included in Figure 2 are the corresponding H_2 adsorption data for CZ-MO, CZ-SO, and CZ-SO-H1223. The relationship existing between the low-temperature redox response, as deduced from Table 1, and the behavior of the oxides against hydrogen chemisorption, Figure 2, seems clear. If CZ-MO and CZ-MO-O1123 are compared, we may observe the coincidence of high-temperature ($T \geq 973$ K) OSC values, and the remarkable difference existing between their low-temperature ($T \leq 773$ K) redox response, much lower OSC values being determined for the CZ-MO-O1123 sample (Table 1). In parallel with this low-temperature redox effect, the hydrogen chemisorption capability of the CZ-MO-O1123 sample is very significantly deteriorated with respect to that of CZ-MO. The opposite effect may be deduced from the comparison CZ-SO and CZ-SO-H1223 samples. As in the previous case, a coincidence of OSC values at 1223 K now is observed. By contrast, the low-temperature redox response of CZ-SO-H1223 is significantly better than that of CZ-SO (Table 1). In parallel with this latter effect, Figure 2 clearly shows an enhanced hydrogen chemisorption capability for CZ-SO-H1223 as compared to that of CZ-SO. We should conclude accordingly that, with independence of their bulk structural properties, the low-temperature redox response of this series of mixed oxides is mainly determined by their surface structure, this feature being responsible for their chemisorptive behavior against hydrogen and therefore for the kinetics of their low-temperature reduction.

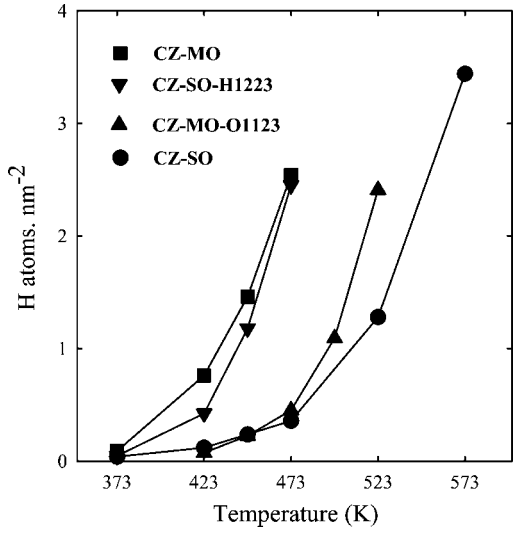

Figure 2. Volumetric study of H_2 chemisorption on CZ-MO, CZ-MO-O1123, CZ-SO, and CZ-SO-H1223. The experiments consisted of heating the samples under H_2 ($P_{H_2} = 38$ Torr), for 30 min, at each of the indicated temperatures, followed by cooling to 298 K under H_2. H_2 adsorption was determined from the pressure drop at 298 K.

HREM and STEM-XEDS Studies. *HREM Studies.* The parallel HREM study fully agrees with the proposal made in the previous paragraph. In effect, Figure 3A,B depicts, respectively, representative images of the CZ-MO and CZ-SO samples. Two major points may be stressed from their comparative analysis. First, there is the obvious difference in face developments, with the inherent change in the external morphology of the microcrystals.[20,22] Second, there is the observation in the HREM image of the CZ-MO sample (Figure 3A) of the very characteristic superstructure contrasts due to the pyrochlore-related phase, with lattice spacings double those of the primitive fluorite structure from which it is derived.[16,20] These specific contrasts correspond to the 1/2 {111} superstructure spots in the DDP included as the inset in Figure 3A. As deduced from the HREM image and inset DDP in Figure 3B, these features hardly are observed in the case of CZ-SO. Within the range of experimental thermal aging conditions investigated in this work, Figure 3A,B accounts, respectively, for the starting (ordered) and final (disordered) states of the process of destruction of the pyrochlore-related mixed oxide phase.

Regarding the HREM study reported in Figure 3C,D, there are two major aspects to be outlined. First, both HREM images and corresponding DDPs clearly show that the samples resulting from the short oxidizing treatment of CZ-MO at 1073 and 1123 K mainly consist of a pyrochlore-related ordered phase. The only, very subtle, difference between them and the original CZ-MO sample is the development of a surface roughness affecting a few surface layers. Occasionally, the HREM images recorded for CZ-

(29) Norman, A.; Perrichon, V.; Bensaddik, A.; Lemaux, S.; Bitter, H.; Koningsberger, D. *Top. Catal.* **2001**, *16*−*17*, 363.
(30) Gennari, F. C.; Montini, T.; Hickey, N.; Fornasiero, P.; Graziani, M. *Appl. Surf. Sci.* **2006**, *252*, 8456.
(31) Gatica, J. M.; Baker, R. T.; Fornasiero, P.; Bernal, S.; Blanco, G.; Kaspar, J. *J. Phys. Chem. B* **2000**, *104*, 4667.
(32) Collins, S. E.; José, M.; Cíes, J. M.; del Río, E.; López-Haro, M.; Trasobares, S.; Calvino, J. J.; Pintado, J. M.; Bernal, S. *J. Phys. Chem. C* **2007**, *111*, 14371.

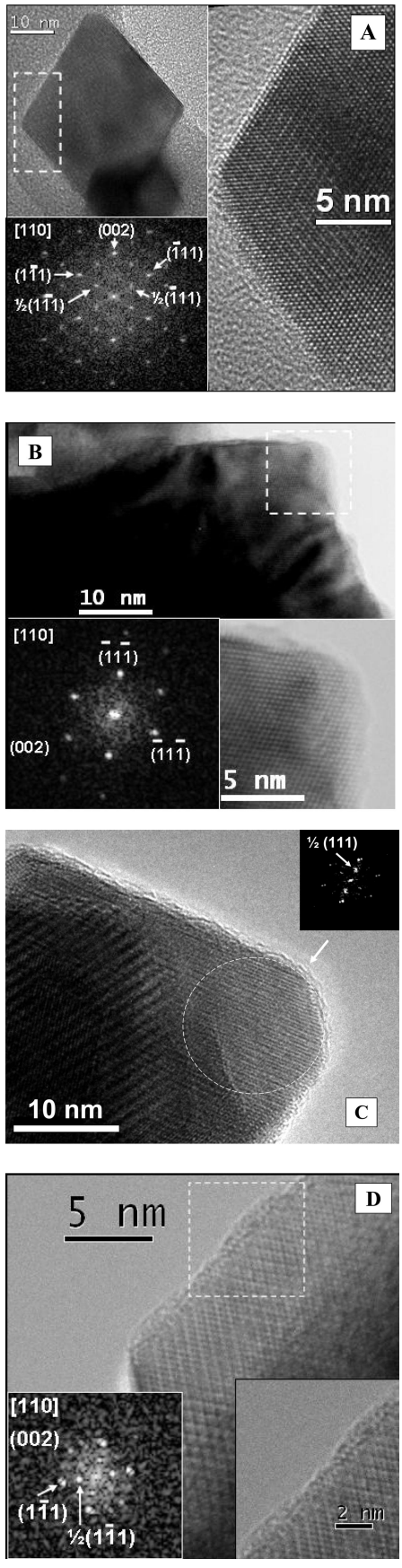

Figure 3. Representative HREM images corresponding to CZ-MO (A), CZ-SO (B), CZ-MO-O1073 (C), and CZ-MO-O1123 (D) oxide samples. The spots in the DDPs included as insets were indexed on the basis of the fluorite structure. The 1/2 (111) reflections at 0.62 nm observed in panels A, C, and D are characteristic of a pyrochlore-related superstructure (ordered Ce−Zr sublattice). These reflections are absent in the DDP of panel B.

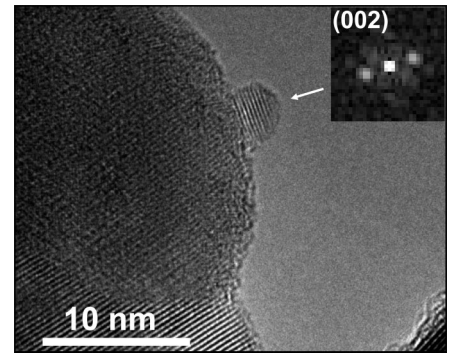

Figure 4. HREM micrograph showing a small globular nodule occasionally observed at the surface of CZ-MO after 30 min oxidizing treatment at either 1073 or 1123 K. The reported image corresponds to CZ-MO-O1073.

MO-O1073 and CZ-MO-O1223 also show the occurrence of small globular nodules at their surface. An example of this phenomenon is reported in Figure 4. The very peculiar nanostructural effects shown in Figures 3C,D and 4 are representative features of the surface rearrangement phenomena occurring at the earliest steps of the destruction of the ordered Ce−Zr sublattice.

As a number of authors have stressed,[19,21] under oxidizing conditions, the pyrochlore-related phase resulting from a high-temperature reduction treatment is thermodynamically unstable against the transition leading to an oxide with a disordered distribution in its cationic sublattice and finally to segregated ceria- and zirconia-rich phases.[33,34] Therefore, the preparation of an ordered phase can only be achieved by mild reoxidation of the heavily reduced oxide (i.e., under conditions at which the rate of the order−disorder process is negligible), as is the case of the MO routine applied in this work. If the metastable ordered phase is heated at high enough temperatures, under oxygen partial pressure allowing the oxide to be kept in a fully oxidized state,[35,36] the ordered phase decomposes. Our results show that this process starts at ca. 1073 K, it being rather slow even at 1123 K.

STEM-XEDS Studies. The STEM-XEDS study shown in Figure 5 provides some additional interesting pieces of information. Figure 5, in effect, summarizes the nanoanalytical data corresponding to a series of XEDS studies carried out on CZ-MO, CZ-SO, and CZ-MO-O1073. Remarkable differences may be noticed from one oxide to the other. In accordance with Figure 5, CZ-MO shows the narrowest compositional distribution, with most of the analyzed nanoregions exhibiting Ce/Zr molar ratios close to the nominal value, 62:38. By contrast, the sample resulting from the high-temperature oxidizing aging treatment, CZ-SO, shows the broadest range of Ce/Zr values. This observation suggests the occurrence of a compositional segregation, a process that is known to be induced on oxides with Ce/Zr molar ratios typically ranging from 50:50 to 70:30, by thermal aging (*T*

(33) Colón, G.; Pijolat, M.; Valdivieso, F.; Vidal, H.; Kaspar, J.; Finocchio, E.; Daturi, M.; Binet, C.; Lavalley, J. C.; Baker, R. T.; Bernal, S. *J. Chem. Soc., Faraday Trans.* **1998**, *94*, 3717.
(34) Colón, G.; Valdivieso, F.; Pijolat, M.; Baker, R. T.; Calvino, J. J.; Bernal, S. *Catal. Today* **1999**, *50*, 271.
(35) Shah, P. R.; Kim, T.; Zhou, G.; Fornasiero, P.; Gorte, R. J. *Chem. Mater.* **2006**, *18*, 5363.
(36) Zhou, G.; Shah, P. R.; Kim, T.; Fornasiero, P.; Gorte, R. J. *Catal. Today* **2007**, *123*, 86.

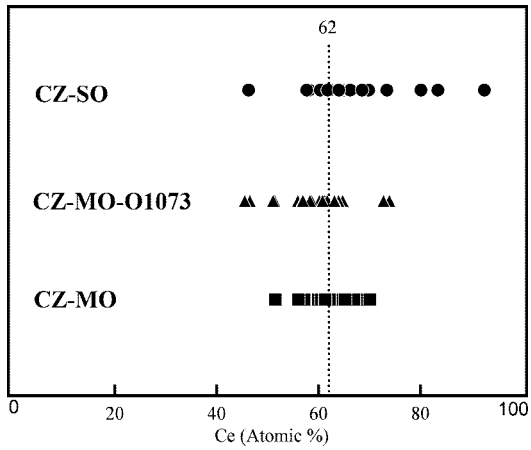

Figure 5. XEDS study of Ce−Zr distribution in CZ-MO, CZ-SO, and CZ-MO-O1073 oxide nanocrystals. Data expressed as atomic percentage of Ce: 100[Ce/(Ce + Zr)].

> 1173 K), under oxidizing conditions.[33,34] In accordance with the X-ray diffraction study reported in ref 33, the segregation process leads to the formation of two new phases that could be indexed as ceria−zirconia solid solutions of approximate compositions Ce/Zr = 80:20 and Ce/Zr = 20:80. As noted in ref 33, however, for an oxide with Ce/Zr = 50:50, a prolonged (140 h) calcination at 1473 K was required to complete the process. In the case of Ce/Zr = 68:32, even higher temperatures are required.[33] Very likely, our CZ-SO sample, which was aged under oxygen at 1223 K, for 5 h, does not represent a true equilibrium state for the system but a transient intermediate situation in a way through the final fully segregated state.

The wideness of the compositional distribution determined for CZ-MO-O1073, although closer to that of CZ-MO, is in between those reported in Figure 5 for CZ-MO and CZ-SO. We should conclude, accordingly, that CZ-MO-O1073 might well correspond to the very first stages of the process transforming the CZ-MO oxide (i.e., the sample mainly consisting of an ordered Ce−Zr sublattice, with a high compositional homogeneity) into two, Ce- and Zr-rich, segregated phases.

The nanoanalytical study commented on previously therefore allows us to propose the existence of a relationship between nanostructural constitution (order/disorder in the Ce−Zr sublattice), compositional homogeneity, and redox properties of the investigated materials. As deduced from our results, the higher the compositional homogeneity, corresponding to the ordered pyrochlore-related phase, the higher the reducibility of the oxide. This conclusion is in fairly good agreement with that proposed in ref 37 on the basis of EXAFS data. By contrast, the nanoanalytical study reported in ref 11 led the authors to the opposite conclusion. Most likely, the origin of the disagreement is due to the strong heterogeneity of the starting oxide material. Likewise, the aging and redox evaluation routines followed in ref 11 also may explain the lack of coincidence with the results reported here.

Conclusion

The results reported in this work allowed us to characterize some key chemical, nanostructural, and nanoanalytical features of a ceria−zirconia sample formed at the first stage of the CZ-MO → CZ-SO (order → disorder) phase transition process. If these results are jointly analyzed with those reported in refs 16, 20, and 22, a description of the four major ceria−zirconia states characterizing the chemical and nanostructural structural evolution undergone by the oxide throughout the whole redox aging cycle can be gained. Some key features of this comprehensive model are summarized in Scheme 1.

Scheme 1. Key Features of Model Correlating Thermal Aging Conditions, Nanostructural Properties, Surface Chemistry, and Redox Behavior in Ceria−Zirconia Mixed Oxides

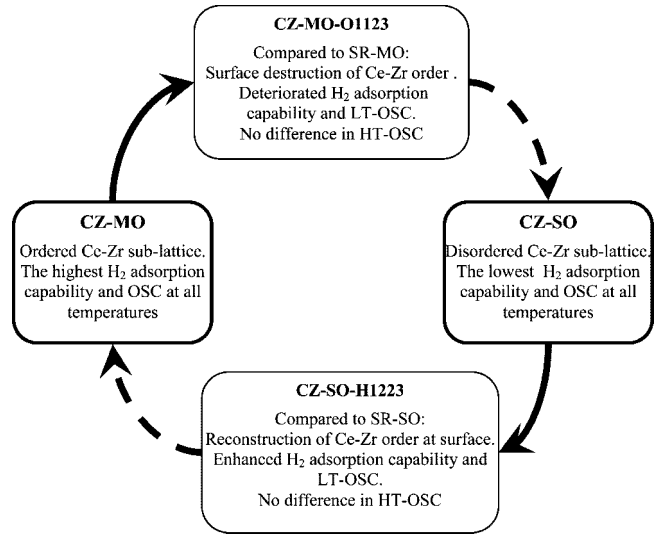

A number of relevant conclusions can be drawn from the analysis of this scheme. The redox response of ceria−zirconia mixed oxides, as revealed by the series of ultimate OSC data recorded at temperatures ranging from 473 to 1223 K, critically depend on their nanostructure and, more specifically, on the order−disorder exhibited by their cationic sublattice.

There is a double, substantially different in nature, influence of the nanostructure on the redox behavior of the oxides. At low temperatures ($T \leq 773$ K), this behavior is mainly determined by the kinetics of hydrogen activation, therefore controlled by the surface structure of the mixed oxide. As deduced from the hydrogen chemisorption studies, the sample showing an ordered pyrochlore-related structure would be the most active sample. This surface state is obviously observed in CZ-MO (i.e., that mainly consisting of an ordered structure both at the surface and in the bulk of the oxide), but it also occurs in CZ-SO-H1223.[20] In accordance with the results reported in Table 1, the influence of the surface properties also may be observed in the opposite sense. If an oxidizing aging pretreatment at 1073 or 1123 K is applied to CZ-MO, the sample exhibiting the highest redox activity at all temperatures, a significant loss of its low-temperature OSC is observed. According to the suggested model, this perturbation of oxide reducibility would reflect the structural changes occurring at the surface of the CZ-MO sample with inherent deterioration of its hydrogen activation capability.

In the domain of high temperatures ($T \geq 973$ K), the OSC data are mainly determined by the thermodynamic properties of the oxides (i.e., by structural properties of their bulk). Accordingly, CZ-MO, CZ-MO-O1073, and CZ-MO-O1123, all of them consisting of an ordered bulk structure only differing in their surface properties, show very similar high-temperature OSC data. Likewise, CZ-SO and CZ-SO-H1223, those having in common their disordered bulk structure,[20] although different surface structures, exhibit very close high-temperature OSC values.

This double dependence, kinetics in the low-temperature range and thermodynamics in the high-temperature domain, is critically important to fully understand the complex effect of different thermal aging pretreatments on the redox behavior of these materials. Moreover, on the basis of this model, the very strong dependence of the redox response on the previous history of a certain ceria−zirconia mixed oxide can be reasonably interpreted.

Since the usually applied thermal aging pretreatments do not lead to true equilibrium states of the oxides, the extent of the rearrangements induced in the bulk and/or surface cationic substructure can hardly be quantified, thus allowing us to understand the variable and very puzzling effect of different series of aging pretreatments. The proposed model strongly suggests that processes implying the formation/destruction of an ordered Ce−Zr sublattice start at the surface of the oxide, their progress being very much dependent on the applied aging conditions (redox balance of the chemical environment as well as temperature and duration of the aging pretreatment). We also deduce from the reported results that these processes require temperatures of or above 1073 K.

As revealed in the HREM studies, the structural changes associated with the occurrence of significant modifications in the low-temperature redox response of these oxides are very subtle. They typically affect a few surface layers, therefore hardly are detected by most of the experimental techniques commonly used in the characterization of these materials. Such is the case of X-ray diffraction,[1,2,5,6,21,23] Raman spectroscopy,[2,6,15,19,21,38] or EXAFS.[37–39] This is certainly an additional reason contributing to the very challenging nature of the discussed phenomena.

Scheme 1 also shows that analysis of the thermal aging−nanostructure−redox behavior correlation should be made on the basis of OSC data recorded throughout the whole range of reduction temperatures. Otherwise, very misleading conclusions may be drawn. Moreover, the effect of a specific pretreatment on both low- and high-temperature OSC data may allow us to deduce as to whether the structural modifications induced by the applied pretreatment consist of a surface phenomenon or also affect the bulk of the ceria−zirconia mixed oxide. In the first case, the aging pretreatment only modifies the low-temperature response, whereas in the latter, both low- and high-temperature OSC data are altered.

Acknowledgment. We thank the Ministry of Education and Science of Spain/FEDER Program of the EU (Project MAT2005-00333) and the Junta de Andalucı´a (Groups FQM-110 and FQM-334) for financial support. The ceria−zirconia mixed oxide used as a starting material was kindly donated by Grace Davison Company. Nanostructural and nanoanalytical studies were performed at the electron microscopy facilities of the University of Cádiz.

CM800928P

(37) Nagai, Y.; Yamamoto, T.; Tanaka, T.; Yoshida, S.; Nonaka, T.; Okamoto, T.; Suda, A.; Sugiura, M. *Catal. Today* **2002**, *74*, 225.
(38) Si, R.; Zhang, Y.-W.; Wang, L.-M.; Li, S.-J.; Lin, B.-X.; Chu, W.-S.; Wu, Z.-Y.; Yan, C.-H. *J. Phys. Chem. C* **2007**, *111*, 787.
(39) Lemaux, S.; Bensaddik, A.; van der Eerden, A. M. J.; Bitter, J. H.; Koningsberger, D. C. *J. Phys. Chem. B* **2001**, *105*, 4810.